PCCP

Zinc-containing porphyrin aluminum MOF in sorption of diethyl sulfide vapor: Mechanistic experimental and computational study

Journal:	*Physical Chemistry Chemical Physics*
Manuscript ID	CP-ART-08-2023-003779.R1
Article Type:	Paper
Date Submitted by the Author:	28-Oct-2023
Complete List of Authors:	Ullah, Shaheed; Morgan State University, Department of Chemistry McKee, Michael; Auburn University, Department of Chemistry and Biochemistry Samokhvalov, Alexander; Morgan State University, Department of Chemistry

Zinc-containing porphyrin aluminum MOF in sorption of diethyl sulfide vapor: Mechanistic experimental and computational study

Shaheed Ullah [1], Michael L. McKee [2], and Alexander Samokhvalov [1]*

[1] Department of Chemistry, Morgan State University, 1700 East Cold Spring Lane, Baltimore, MD 21251, USA.

[2] Department of Chemistry and Biochemistry, 179 Chemistry Building, Auburn University, Auburn, AL 36849, USA.

*** The corresponding author.**

Abstract
We report mechanistic study of interactions in sorption of volatile organic sulfur compound (VOSC) diethyl sulfide (DES) by zinc porphyrin aluminum MOF (actAl-MOF-TCPPZn) compound 3. First, interactions were studied under dynamic conditions with vapor of DES in flowing air, using *in-situ* time-dependent ATR-FTIR spectroscopy in controlled atmosphere with new facile spectroscopic mini-chamber. The first binding site includes μ(O-H) and COO^- groups as detected by characteristic peak shifts. Control experiments with model compound, which lacks porosity and these groups, show no peak shifts. An additional insight was obtained by DFT computations using small clusters. Kinetics of sorption of DES by compound 3 is of Langmuir adsorption model and pseudo-first order with rate constant $r_{obs} = 0.442 \pm 0.056$ min^{-1}. Sorption of DES under static conditions in saturated vapor results in stoichiometric adsorption complex $[Al\text{-}MOF\text{-}TCPPZn]_1(DES)_4$ characterized by spectroscopic, structural and gravimetric methods; adsorbed amount is very high (381 mg/g sorbent). The repetitive sorption and desorption of DES is conducted, with facile regeneration. Finally, mechanistic detail was targeted by Raman and photoluminescence (PL) spectroscopy by confocal Raman microscope. Photoexcitation of compound 3 at 405 nm into the Soret band of metalloporphyrin linker shows the characteristic PL peaks of Q-bands: the purely electronic Q(0-0) and first vibronic Q(0-1) band. Upon interaction with DES, preferential quenching of PL from the Q(0-0) band occurs with significant increase of signal of vibronic Q(0-1) band, reflecting bonding to metalloporphyrin ring. Compound 3 is of interest to mechanistic studies of VOSCs, their removal from air, and optical chemo-sensing.

Keywords: metal-organic framework; diethyl sulfide; sorption; controlled atmosphere; ATR-FTIR; in-situ; time-dependent; DFT; kinetics; photoluminescence

1) Introduction

Volatile organic sulfur compounds, VOSCs are toxic with noxious smell and they are hazardous chemicals [1]. VOSCs originate in raw products and off-gases of petroleum and natural gas industry and microbial decomposition of organic matter [2]. Among VOSCs, diethyl sulfide DES (Figure 1) is an archetypal compound of simple molecular structure, which is commonly found in products and by-products of processing petroleum and natural gas [3].

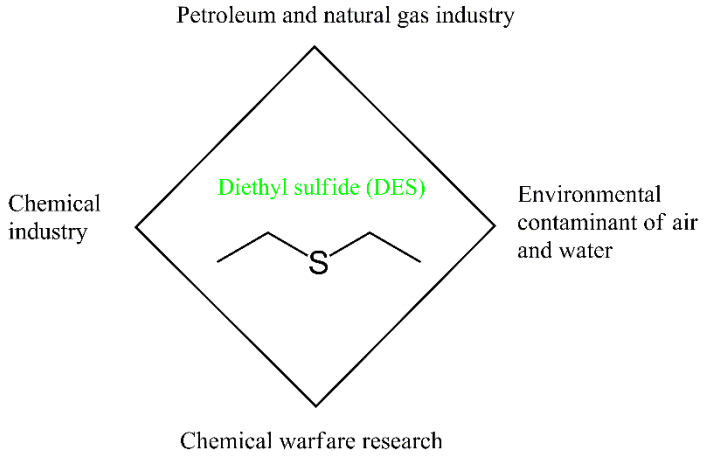

Figure 1. Molecular structure and uses of diethyl sulfide (DES).

Air contamination with DES originates in landfills [4] and agricultural facilities [5]. DES finds applications as solvent, in synthesis of chemicals, and as surrogate compound of major chemical warfare agent sulfur mustard, SM [6]. Sulfur mustard is extremely toxic and research with it can only be conducted at specialized facilities [7]. DES is much less toxic than SM and is suitable for research at universities as a surrogate SM and potential CWA. There are only very few studies of sorption of DES; an experimental study [8] reports sorption of DES vapor in air on "conventional" sorbent activated carbon. Computational studies of sorption of DES are also very rare and limited to zeolites [9]. There is a surge of interest in "unconventional" sorbents, which synergistically combine ultra-high porosity with inorganic and organic groups as binding sites.

Metal-organic frameworks (MOFs) are nano-porous coordination polymers consisting of metal sites and organic linkers. MOFs are "hot spot" in research and industrial applications in separations [10], environmental remediation [11], sensing [12], catalysis [13]. MOFs feature very large nanopore volumes and areas, plus their metals and/or linkers serve as binding sites for interaction with adsorbates. MOFs are widely investigated for sorption of gases and vapors of hazardous compounds and industrial chemicals [14] such as NH_3, SO_2, NO_2, H_2S and chemical warfare agents [15]. To our knowledge, there are no studies of sorption of diethyl sulfide by any MOF.

Aluminum MOFs (Al-MOFs) are highly promising for sorption in solution [16] and gas phase [17]. Al-MOFs show outstanding stability at high temperatures and in highly aggressive environments [18]. Porphyrins are group of nitrogen heterocyclic compounds which, for decades, have found multiple uses in research [19]. Derivatives of tetrakis(4-carboxyphenyl)porphyrin $TCPPH_2$ are highly stable in aggressive environments, e.g. photocatalytic water splitting [20]. Their attractive properties are often retained when these compounds are used as linkers in MOFs; porphyrin MOFs are of interest as chemo-sensors [21] and sorbents [22]. Further, one can enhance structural versatility of porphyrin MOFs by inserting metal cation to the porphyrin ring of their linker [23]. The obtained highly advanced materials, for example, zinc-containing porphyrin aluminum MOFs, are expected to have an exceptionally diverse set of functional groups: the highly polar OH group, the weakly

polar pyrrole ring, and TM (Zn^{2+}) cation. Hence, these nanomaterials are capable of interactions with various "guest" molecules by variety of molecular mechanisms.

The mechanism of bonding and structure of binding site are often studied by spectroscopic analysis [24]. The infrared (IR) spectroscopy is well suitable for detection of adsorbates, and it also allows determination of mechanistic detail of binding [25] for the sorbent and/or adsorbate. Attenuated total reflection Fourier transform infrared (ATR-FTIR) spectroscopy uses optical geometry, where the evanescent field of IR radiation is in direct contact with sample. The *in-situ* modality of ATR-FTIR spectroscopy allows studies of sorption mechanism, by the micro-reactor furnished as part of the IR spectrometer e.g. [26]. When *in-situ* ATR-FTIR spectra are progressively recorded in time, this is denoted *in-situ* time-dependent ATR-FTIR spectroscopy. Surprisingly, there are very few studies of sorption by porous materials in the form of powder using *in-situ* time-dependent ATR-FTIR spectroscopy [27]. Controlled atmosphere allows eliminating adverse effects of dust and ambient compounds e.g. water vapor, oxygen, carbon dioxide and protects operator from toxic gases; this finds use in work with hazardous materials [28]. Recently, we reported *in-situ* time-dependent ATR-FTIR spectroscopic study of mechanism of sorption and desorption of water vapor on molecular sieves [29], using a custom-built flow chamber in shape of large box (height of 7 inches and width of 9 inches) attached to the ATR-FTIR spectrometer.

To our knowledge, there are no reports of sorption of VOSCs by using *in-situ* ATR-FTIR spectroscopy in controlled atmosphere. Herein, we report the following. First, we studied the interaction of aluminum porphyrin MOF compound 3 actAl-MOF-TCPPZn, Figure 2 (its 3D structure is in ref. [30] as Figure 4c; all Al centers are octahedral and each Al atom is coordinated by six oxygen atoms) with vapor of DES. This interaction was investigated in flowing dried air, using *in-situ* time-dependent ATR-FTIR spectroscopy in controlled atmosphere. Here, the significantly improved spectroscopic mini-chamber ATR-FTIR accessory is described and tested, which has an internal volume for reactants of only few cubic millimeters.

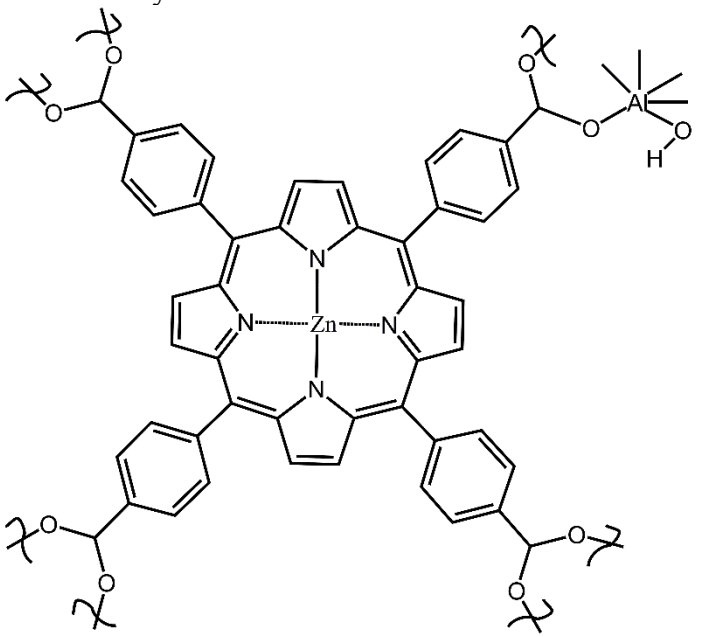

Figure 2. Simplified structure of zinc-containing porphyrin aluminum MOF compound 3 (actAl-MOF-TCPPZn).

Second, we identified specific binding sites in compound 3 that react with DES molecules, using *in-situ* time-dependent ATR-FTIR spectroscopy in controlled atmosphere with this mini-chamber. Third, quantum chemical modeling by DFT computations was conducted to get insight on binding sites. Fourth, chemical kinetics of sorption of DES vapor by compound 3 was determined. Fifth, sorption of DES vapor was studied in static (equilibrium) conditions in saturated vapor, and formation of stoichiometric adsorption complex was assessed by spectroscopic, structural and gravimetric methods. Sixth, repetitive adsorption and desorption of DES vapor was investigated. Finally, interaction of DES vapor with compound 3 was assessed by Raman spectroscopy and by novel method - photoluminescence (PL) spectroscopy conducted by confocal Raman instrument.

2) Materials and Methods

2.1) Chemicals

Precursor of the non-activated form of porphyrin metal-organic framework Al-MOF-TCPPH_2 without zinc was tetrakis(4-carboxyphenyl)porphyrin (abbreviated TCPPH_2) of ≥97.0% purity (from TCI). Another precursor was aluminum chloride $AlCl_3 \cdot 6H_2O$ of 99 % purity (from Alfa Aesar). N,N-dimethylformamide (DMF) of ≥99.5% purity was from TCI, and acetone of reagent purity was from Electron Microscopy Sciences. For insertion of zinc into compound 2, anhydrous zinc acetate $Zn(CH_3COO)_2$ was used of 99.95% purity (from Beantown Chemical). Finally, diethyl sulfide (DES) was of >98.0% purity from TCI.

2.2) Synthesis of actAl-MOF-TCPPZn (compound 3)

Compound 3 was prepared by post-synthetic modification of activated form of Al-MOF-TCPPH_2 (compound 2) First, non-activated form asisAl-MOF-TCPPH_2 (compound 1) was prepared by autoclave method [25] and then was activated at 200 °C in vacuum for 20 h. to yield activated form actAl-MOF-TCPPH_2 (compound 2). Compound 2 was stored in a jar sealed with Parafilm. Second, insertion of Zn^{2+} to compound 2 was conducted similarly to ref. [30], with modifications. Briefly, working in a glove bag, 87 mg (0.1 mmol) compound 2 was mixed with 18.3 mg (0.1 mmol) anhydrous zinc acetate and 5 ml DMF in a 30 ml reactor vial (from Biotage, product 356290), mini stir bar was added, and reactor vial was capped with PTFE lined cap. Reactor vial was heated in an oil bath under magnetic stirring at 100 ℃ overnight. The obtained powder was filtered, washed excessively with DMF until filtrate was colorless, and then with acetone to remove DMF. Finally, the obtained asis Al-MOF-TCPPZn was activated in vacuum at 200 ℃ for 20 hours, to yield target compound 3 actAl-MOF-TCPPZn which was stored in closed jar sealed with Parafilm.

2.3) Characterization of samples

FTIR spectra were collected using Nicolet IS10 spectrometer in ATR-FTIR mode. The spectrometer was equipped with an ATR accessory (Golden Gate, from Specac, part number GS10500) with diamond ATR crystal. The software program for data acquisition was OMNIC; and optical aperture was set “Open”, and spectral resolution was set at 4 cm^{-1}.

To avoid potentially adverse effects of water vapor in ambient air on the spectra, FTIR spectrometer has been continuously purged with dried air at rate 30 scfh (standard cubic feet per hour) measured by flowmeter (Dwyer RMA-7). Dried air was produced by an FT-IR purge gas generator (model 74-5041 from Parker Balston). The remaining water vapor content in dried air, per manufacturer, corresponds to dewpoint of -100 ℉ (-73 ℃) and relative humidity RH <1%. This purge gas generator also removes carbon dioxide from air to <1 ppm. To continuously monitor quality of FTIR spectra and remove artifacts due to trace water vapor, OMNIC data acquisition software had “Atmospheric Correction” parameter enabled, and “Spectral Quality

Results" parameter set at "H_2O level" ≥95 %. The ATR-FTIR spectra were plotted in absorbance mode. Numeric peak fitting of IR spectra was conducted using Microcal Origin 2016 program.

Powder X-Ray diffraction (XRD) traces were collected by diffractometer Rigaku MiniFlex with X-rays at the Cu K-alpha line of 0.15418 nm and the increment of 2θ angle was 0.02 deg.

The Raman spectra were collected using confocal Raman microscope model XploRA Plus from Horiba Scientific. Magnification of objective was x50 and the 405 nm laser was used at 1% of maximum power. A small amount of compound 3 was placed on microscope glass slide, covered with thin microscope glass cover slide, and Raman spectra were collected. In work with DES, a small amount of compound 3 was placed on microscope glass slide, wetted with few drops of DES, covered with thin microscope glass cover slide, and Raman spectra collected in the range 70-2000 cm^{-1}. The photoluminescence (PL) spectra were collected using the same confocal Raman microscope XploRA Plus, with the same settings, but in the much wider range of 70-12,200 cm^{-1} and subsequently were re-plotted to the wavelength (nm) scale. Numeric peak fitting was conducted using Microcal Origin 2016 program.

2.4) Hemi-spherical gas flow spectroscopic mini-chamber for *in-situ* time-dependent ATR-FTIR spectroscopy in controlled atmosphere

Home-built hemi-spherical gas flow spectroscopic mini-chamber attachment is denoted "spectroscopic mini-chamber" for convenience. Figure 3 shows it installed on top of baseplate of ATR assembly (from Specac, section 2.3) of FTIR spectrometer Nicolet IS10. Specifically, in Figure 3 the spectroscopic mini-chamber in shape of hemi-sphere is placed on top of spectrometer baseplate (item 1, rectangle) which includes the ATR plate with diamond ATR crystal. The specimen (item 2, red circle) is pressed to the ATR crystal by the ATR anvil (item 3, gray cone). Item 4 is a gas inlet port and item 5 is a gas outlet port.

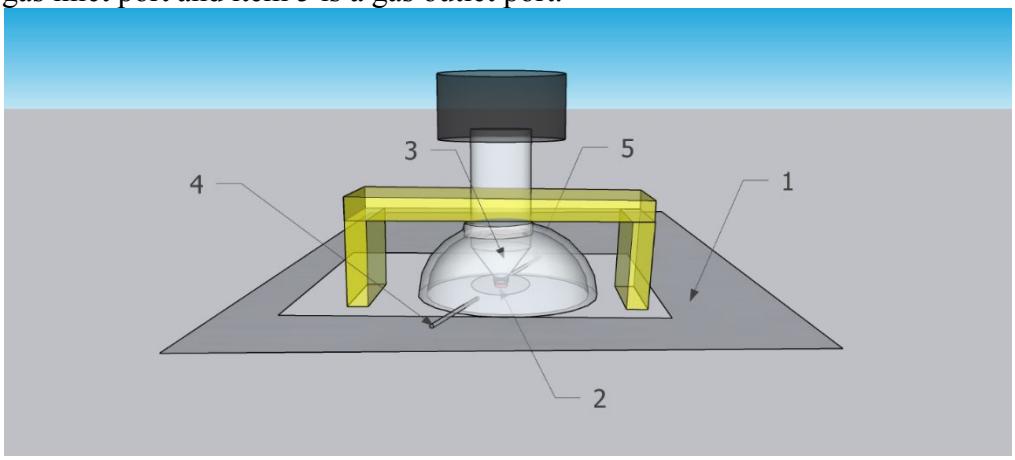

Figure 3. Schematics of spectroscopic mini-chamber installed on baseplate of FTIR spectrometer with pre-installed ATR assembly.

The bridge of the ATR assembly (yellow) is above the spectroscopic mini-chamber and it presses it down when engaged. The screw of the ATR assembly (white cylinder) protrudes inside the spectroscopic mini-chamber via its top opening, and this top screw knob is also part of standard ATR assembly. The ATR screw assembly is shown lowered, with ATR anvil (model Specac product 10531) firmly pressing powdered specimen to the ATR crystal.

The drawing in Figure 3 was made using SketchUp Pro 2022 program.

2.5) Dynamic sorption of DES by compound 2, using *in-situ* time-dependent ATR-FTIR spectroscopy in controlled atmosphere

The flow of dried air (as carrier gas) was prepared by the FT-IR Purge Gas Generator (model 74-5041 Parker Balston) at RH<1%. The obtained stream of dried air was reduced to flow rate at 100 ml/min. using Dual Flowmeter (TA Instruments part 270134.002) and passed to the inlet of the spectroscopic mini-chamber. For generation of the flow of vapor of DES in dried air, a simple in-flow vapor saturation setup was constructed as in Figure S2. The simple in-flow setup was a 50 ml Büchner flask about ½ filled with liquid DES. The flask had a stopper with glass Pasteur pipette, one end of which was connected to ¼ inch flexible pipe (inlet), and the other end was protruding to bottom of flask, below surface of liquid DES. The flow of dried air was passed through the in-flow setup at flow rate of 100 ml/min, and the obtained stream of vapor of DES in dried air was directed to the inlet port of the spectroscopic mini-chamber DES is a volatile liquid (boiling point 92 °C) which creates vapor pressure of 60.2 mm Hg at 25 ℃ (from Hazardous Substance Fact Sheet, NJ, USA). Vapor pressure of DES in flowing dried air is less than its thermodynamic equilibrium vapor pressure at the same temperature.Prior to the start of dynamic *in-situ* sorption experiment, a small sample (few mg) of compound 3 was placed on the ATR crystal. Promptly, the spectroscopic mini-chamber was placed on the ATR base plate (Figure 3), so that its anvil was in contact with specimen on the ATR crystal. Then, the locking mechanism of the ATR assembly was engaged pressing the ATR anvil to the specimen on the ATR crystal, and the sample was ready to exposure by the flowing gas.

To measure spectra of pure compound 3, dried air was passed through the spectroscopic mini-chamber, and a few reference ATR-FTIR spectra were collected; each spectrum was averaged 64 times (96 sec or ca. 1.6 min.). Then, the flow of gas through the spectroscopic mini-chamber was changed to purge gas (dried air saturated with vapor of DES) at the same flow rate 100 ml/min. The *in-situ* time-dependent ATR-FTIR spectra were collected sequentially with the same settings.

2.6) Static sorption (no flow) of saturated DES vapor in dried air by compound 3

Sorption of DES vapor was conducted in a simple vapor saturation chamber (closed glass desiccator) similar to that described by us [25] for sorption of water vapor. The modifications were: a) the vapor saturation chamber did not contain hygrometer/thermometer, b) instead of liquid water, liquid DES was used, c) immediately before inserting the sample, the interior of vapor saturation chamber has been purged with dried air, d) then the pre-weighted sample of compound 3 on a quartz XRD sample plate was inserted into the vapor saturation chamber. Then, the vapor saturation chamber was tightly closed and left overnight at room temperature. The obtained sorption complex with nominal formula $[\text{Al-MOF-TCPPZn}]_x[\text{DES}]_y$ was denoted adsorption complex compound 4. Compound 4 on a quartz plate was removed from the vapor saturation chamber, promptly weighted, returned to the chamber, and stored in it. For ex-situ analysis, compound 4 on a quartz XRD plate was transferred to the sample compartment XRD instrument.

2.7) Periodic static sorption and desorption of DES vapor by compound 3

In static sorption/desorption tests of DES vapor, the "spent" sorbent (aka adsorption complex) compound 4 was re-activated to remove DES adsorbate at 30 °C for 72 hours in the vacuum oven (model AT09e.110 from Across International) connected to a two-stage vacuum oil pump (pumping speed 12 cfm, from Xtractor Depot). Base pressure in the vacuum oven was at <100 mTorr measured by the Convectron gauge and digital controller (Phillips 275). Then, the re-activated sample was promptly weighted, and returned to the same vapor saturation chamber.

2.8) DFT computations

The Gaussian 16 program [31] was used for all geometry optimizations and frequency calculations. The first cluster Al-TCPPZn cluster model was based on our previous work [32] on MIL-53(Al). Here, two benzene-1,4-dicarboxylate dianion linkers in MIL-53(Al) were replaced with two porphyrinZn(-2) rings. The linkers and cluster-terminating HCO_2(-1) and OH(-) groups were distributed to give an average +3 oxidation state for each Al atom. Namely, the cluster modeling sorbent compound 3 is denoted Al-TCPPZn and it contains 308 atoms, see Table S1 below for the number of each group in this model. One negative (-1) charge is required to give an average +3 oxidation state for each Al center.

The second cluster models the product of interaction of sorbent compound 3 with DES molecules (i.e. compound 4) and it consists of cluster Al-TCPPZn plus 2 DES modules. This cluster is denoted 2DES@Al-TCPPZn and it contains 338 atoms. Clusters were optimized with C_2 symmetry at the B3LYP/6-31G(d)+D3BJ level.

3) Results and Discussion

3.1) Characterization of sorbent (compound 3) and adsorbate (diethyl sulfide, DES)

Prior to sorption, a small (few mg) specimen of activated sorbent compound 3 (actAl-MOF-TCPPZn) has been placed on ATR crystal, promptly covered with spectroscopic mini-chamber continuously purged with dried air; the *in-situ* ATR-FTIR survey spectrum is in Figure S3.

Assignments of IR peaks of similar compound 2 *act*Al-MOF-TCPPH_2 are in [25]; the only difference is Zn^{2+} cation in porphyrin ring of linker in compound 3, instead of two -H units in compound 2. Compound 3 does not have N-H bonds in porphyrin ring of linker which is reflected in Figure S3 as absence of N-H peak at ca. 3300 cm^{-1} and major IR peaks are in Table S2.
Peaks at ca. <900 cm^{-1} belong to group frequencies which are difficult to assign to vibrations of one specific functional group, and they are not listed; bonds of Zn are not detectable in IR spectra.

Figure S4 shows powder XRD pattern of compound 3 which is consistent with that in ref. [30]. Numeric analysis of sharp high- intensity peak at 2θ = 14.0 deg. (marked with arrow) was performed by using the Scherrer's equation $D = k\,\lambda / \beta \cos(\theta)$. In this equation, k is a constant (a shape factor with numeric value 1.075 for nanoparticles of spherical shape [33]), λ is an X-ray wavelength, β is the full-width at the half-maximum (FWHM) of diffraction peak of interest (in radian), and θ is the Bragg angle. The Scherrer analysis yields an average nanocrystal size of compound 3 at 48 nm.

Figure S5 shows survey ATR-FTIR spectrum of adsorbate diethyl sulfide DES (in the form of liquid since the ATR-FTIR spectrometer does not allow measurements of vapors). For the sake of comparison, this spectrum is scaled in the same wavenumbers range as the survey spectrum of sorbent compound 3 in Figure S3; Table S3 shows assignments of IR peaks of DES. In Figure S5 spectral range of ca. 3000-2800 cm^{-1} (shaded area) has strong and distinct peaks due to vibrations of C-H bonds in the methyl and methylene groups in DES molecule. In contrast, the ATR-FTIR spectrum of sorbent compound 3 in Figure S3 does not have peaks in this range.

Figure S6 shows ATR-FTIR spectra of DES in three major ranges: a) high wavenumbers, b) mid-IR, and c) low wavenumbers. In Figure S6 there are peaks of DES in mid-IR range and at low wavenumbers, but sorbent compound 3 in Figure S3 also has many peaks in those ranges. It is convenient to detect sorption of DES by compound 3 via monitoring temporal evolution of peaks of DES in 3000-2800 cm^{-1} range, using *in-situ* time-dependent ATR-FTIR spectroscopy in controlled atmosphere (below).

3.2) Mechanism of progressive sorption of DES vapor by compound 3 studied by *in-situ* time-dependent ATR-FTIR spectroscopy in controlled atmosphere

After gas flow has been changed from dried air to purge gas (DES vapor in dried air), the *in-situ* ATR-FTIR spectra of compound 3 have been continuously collected and saved, Figure 4. Each spectrum is an average of 64 scans (1.6 min.) and as time progresses, one can see gradual changes.

Temporal changes in ATR-FTIR spectra can be classified into the following types. The first type of change is growth of peak. The most drastic peak growth is in Figure 4a for the set of four peaks of DES adsorbate within 3000-2850 cm^{-1} (marked with red dashed shape and an up arrow). Specifically, peaks at 2967, 2922, and 2867 cm^{-1} are, respectively, the asymmetric stretch vibration of the CH_2 group, the symmetric stretch vibration of the CH_2 group plus stretch vibration of the CH_3 group, and the symmetric stretch of the CH_3 group, see Table S3. Growth of these peaks indicates progressive increase in quantity of DES adsorbed by compound 3. Additionally, in Figure 4b one can see the concurrent less drastic, but clear growth of other peaks of DES at 1257 cm^{-1} due to wagging vibration of its CH_2 group [34], marked with "Adsorbate" and an up arrow.

The second change is shift of peak; in Figure 4a the peak at 3708 cm^{-1} due to the stretch vibration of free (Al)-O–H group in compound 3 undergoes red shift (shown by arrow). This means that the (Al)-O–H group in MOF compound 3, commonly denoted as the μ(O-H) group, interacts with DES adsorbate molecules. Further, in Figure 4b the peak at 1442 cm^{-1} due to vibration of the carboxylate anion in compound 3 also undergoes spectral red shift (shown by arrow).

Finally, there is a decrease in certain peaks, simultaneously with increase of neighboring peaks. Namely, in Figure 4c the peak at 986 cm^{-1} (due to the deformation vibration of μ(O-H) group) undergoes significant decrease, i.e. transformation of this functional group upon sorption of DES. This is expected, based on red shift of the stretch vibration of the same O-H bond in Figure 4a. At the same time, the neighboring peak at ca. 994 cm^{-1} increases indicating formation of "bonded" form of the μ(O-H) group due to its interaction with DES adsorbate. These diverse changes, which also only affect certain, *rather than all peaks* of sorbent during contact with DES vapor indicate, that only specific functional groups of compound 3 interact with adsorbate molecules.

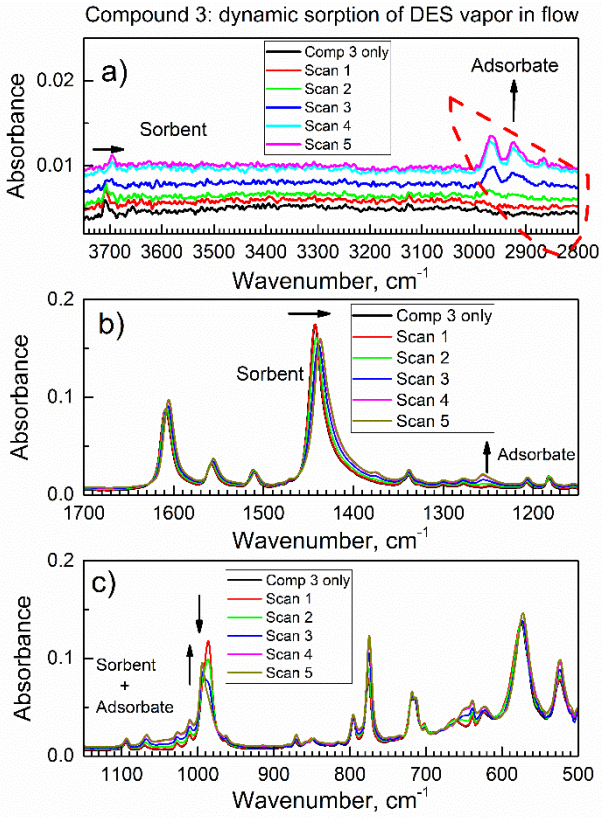

Figure 4. The early period (0-9.6 min) of *in-situ* time-dependent ATR-FTIR spectra of sorbent compound 3 in flow of DES vapor: a) high wavenumbers, b) the mid-IR, c) low wavenumbers.

Figure 5 shows detailed views of time progression of peaks of compound 3 that undergo the most significant changes. In Figure 5b, the magnitude of red shift of peak due to the COO^- group of the sorbent is large: from 1442 cm^{-1} to 1436 cm^{-1} (6 cm^{-1}) which exceeds resolution of FTIR spectrometer at 4 cm^{-1}. Similarly, in Figure 5c, the shift (difference) in peaks of free and bonded μ(O-H) group (994 cm^{-1} – 986 cm^{-1} = 8 cm^{-1}) significantly exceeds the resolution.

During collection of subsequent six *in-situ* ATR-FTIR spectra (9.7-19.2 min.), spectral changes are much less, and spectra stabilize and do not change (data not shown). This illustrates the progress of sorption, and then reaching dynamic equilibrium:

$$[\text{Al-MOF-TCPPZn}]\,(s) + x\ \text{DES}\,(v) \rightarrow [\text{Al-MOF-TCPPZn}](\text{DES})_x\ (s) \qquad (1)$$

where (s) is solid phase, (v) is vapor, and product of interaction is adsorption complex of Al-MOF compound 3 with DES.

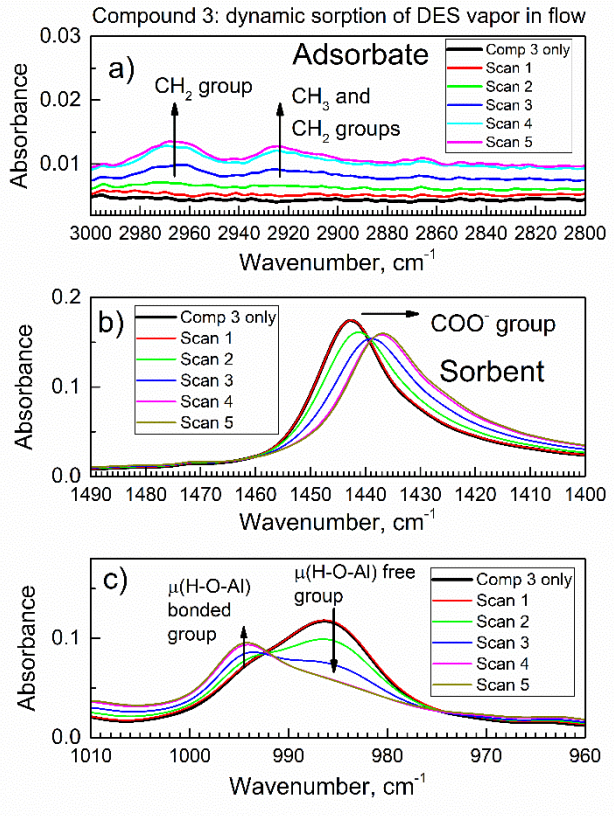

Figure 5. Selected ranges of *in-situ* time-dependent ATR-FTIR spectra of compound 3 in flow of DES vapor in early period of 0-9.6 min. a) the CH_2 and CH_3 peaks of adsorbate; b) the COO^- peak of sorbent; c) the μ(O-H) peak of sorbent.

Data in Figure 4 and Figure 5 indicate that both μ(O-H) and COO^- groups in linker of compound 3 interact with DES molecule, Figure 6.

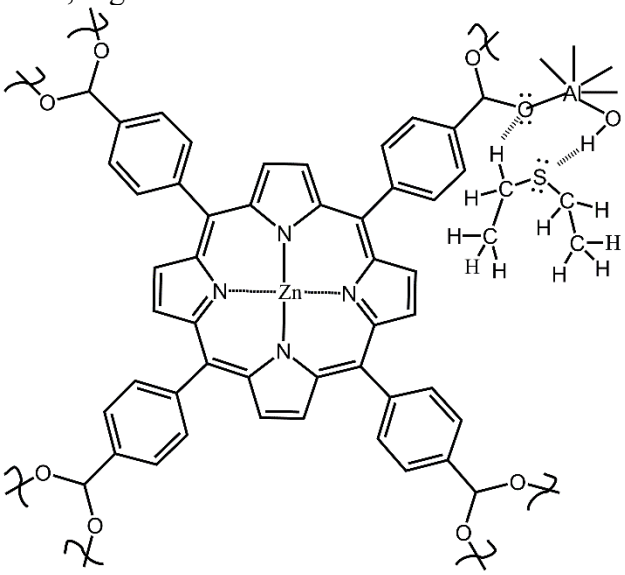

Figure 6. The first (polar) binding site of DES molecule to sorbent compound 3.

The interaction in Figure 6 involves sulfur atom of DES molecule, which has electron lone pairs. The similar intermolecular interactions were described for sorption of organo-sulfur compounds; for example, sorption of dimethyl sulfide on alumina Al_2O_3 with surface hydroxyl groups (Al)-O-H occurs at those groups [35]. For the quantitative assessment of interaction of compound 4 with DES quantum chemical simulations are needed, see section 3.5.

3.3) Assessment of mechanism of sorption of DES vapor by compound 3 with model compound

The sorbent Al-MOF compound 3 features nanoporosity with very large nanopore volume [30] of 3553.1(13) $Å^3$ and it has the μ(O-H) and COO^- groups as binding sites for DES. It is of interest to investigate sorption of DES under similar conditions, but by the model compound of similar structure, except that it does not contain nanopores and the μ(O-H) and COO^- binding groups.

Figure S7 shows such model compound: Zn(II) meso-tetra(4-carboxyphenyl) porphine (ZnTCPP) which is non-porous molecular crystal, with structure resembling the linker of compound 3.

Figure S8 shows the early sequence of *in-situ* time-dependent ATR-FTIR spectra of ZnTCPP model compound collected in flow of DES vapor, with experimental settings and spectral ranges being the same as for Al-MOF compound 3 (see Figure 4 for comparison).

Changes in spectra of ZnTCPP model compound in Figure S7 are much less profound than for sorbent compound 3 in Figure 4. While in Figure S7a there is some growth of absorbance of the C-H peak of DES adsorbate (marked with an arrow), the IR absorbance is much less than that for DES interacting with compound 3. Additionally, there are *no shifts of specific peaks* in spectra of ZnTCPP model; instead, all peaks drift together with spectral baseline. This indicates non-selective and weak interactions between ZnTCPP model compound and DES vapor, while the interaction of DES molecules with porous compound 3 proceeds in its nanopores.

3.4) Modeling of interaction of compound 3 with DES using DFT computations

In order to investigate the interaction of Al-MOF compound 3 with DES adsorbate, we conducted the DFT study using clusters, which mimic major structural features of compound 3 and product of its interaction with DES molecule. For the purpose of modeling, it is important to select the representative cluster; Al-MOF compound 3 (Al-MOF-TCPPZn) has orthorhombic crystal lattice [30], where the secondary building unit (SBU) contains four aluminum atoms in the corners of symmetric nanopore.

The two types of clusters were considered. First, this is the "full cluster" which has the 3D structure of high symmetry and where all functional groups of compound 3 are present. This cluster is denoted Al-TCPPZn, it has 308 atoms total, and its two views are in Figure 7. The Al-TCPPZn cluster of a relatively high symmetry C2 space group models reasonably well the symmetry of orthorhombic lattice of compound 3. Due to symmetry and presence of more than one (Al)-O-H site, that connects SBUs in Al-MOF compound 3, we explored the interaction of Al-TCPPZn cluster with two DES modules. Equation 2 describes computed formal reaction of sorption, where the interaction of DES molecules occurs for the DES-HOAl motif of Al-TCPPZn cluster model of compound 3 (Al-MOF-TCPPZn) compound in this work:

$$2\ \text{DES (g)} + \text{Al-TCPPZn} \rightarrow \text{2DES@Al-TCPPZn} \qquad (2)$$

The resultant cluster labeled 2DES@Al-TCPPZn has 338 atoms total (308 atoms from Al-TCPPZn cluster plus 30 atoms from 2 molecules of DES), and it is in Table 1. The HOAl motif (binding site) of Al-TCPPZn cluster interacting with two DES molecules is shown in Figure 7 (bottom).

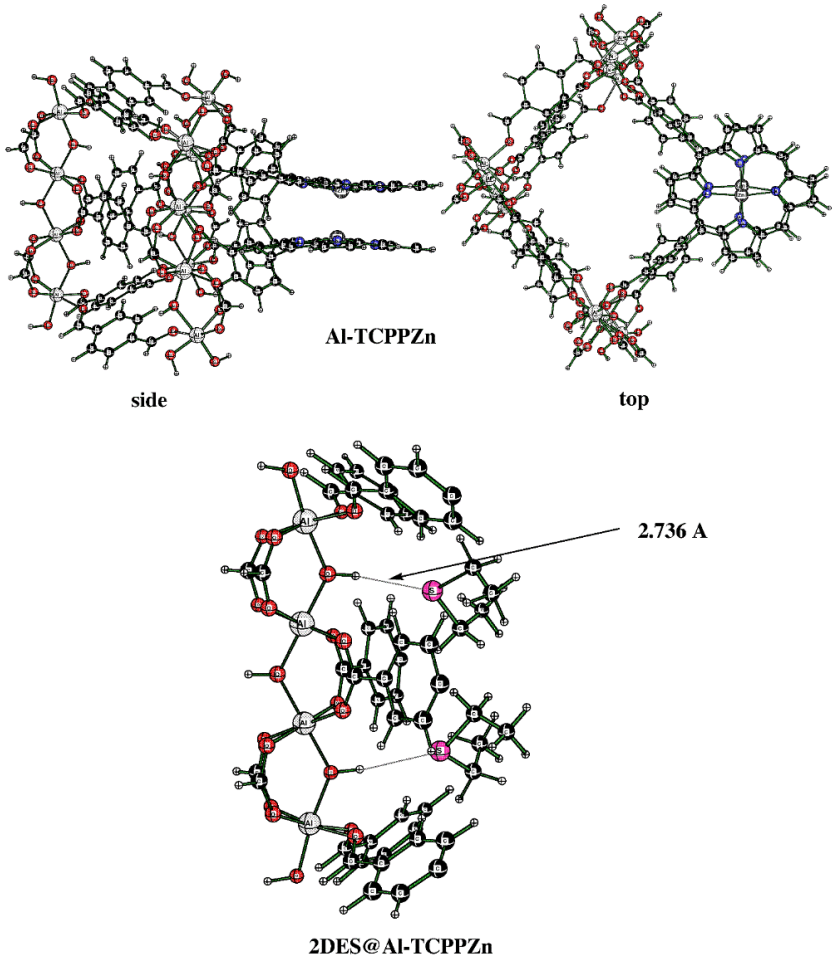

Figure 7. Two views of the Al-TCPPZn model used in the DFT computations. (Top) "full cluster" with a side view and top view; (bottom) side view with most of the atoms not shown so that a clearer view of the two coordinated DES molecules can be seen.

In Figure 7 (bottom), there are two hydrogen bonds from the sulfur atom of DES and the OH group of the Al-TCPPZn model.

Table 1 provides computed parameters of cluster Al-TCPPZn before interaction with two DES molecules, and 2DES@Al-TCPPZn after interaction.

Table 1. Calculated thermodynamic values (kcal/mol) for the Al-TCPPZn model optimized at the B3LYP/6-31G(d)+D3BJ level [a]

Name of cluster	PG	BSSE energy	BSSE-corrected binding energy	Distortion energy	Free energy of binding
Al-TCPPZn	C_2	-	0.0[b]	-	-
2DES@Al-TCPPZn	C_2	4.5	-18.7[b]	2.1	- 6.3

a) Name of cluster, point group (PG), Basis Set Superposition Errors BSSE (per DES molecule), binding energy (per DES molecule) in the Al-TCPPZn model, distortion energy (energy required to distort the model structure to accommodate two DES molecules), and free energy of binding (per DES molecule).

b) The level of theory is B3LYP/6-311G(d,p)+D3BJ//B3LYP/6-31G(d)+D3BJ+BSSE. The binding is for the DES-HOAl motif. The model contains 308 atoms.

The Al-TCPPZn and 2DES@Al-TCPPZn structures were optimized with C_2 symmetry at the B3LYP/6-31G(d)+D3BJ level. The vibration frequency calculation for the 308-atom and 338-atom structures revealed one and three imaginary frequencies, respectively. Because low frequency modes have a large impact on the calculated entropy, the imaginary frequencies were treated as real modes and their contributions were added to the total entropy. The common dispersion correction D3BJ was used as there were a number of intermolecular close-contacts [36].

Table S4 in Electronic Supplementary Information shows Cartesian coordinates of the three clusters: DES molecule denoted "DES al-linker11", cluster modeling compound 3 in this work "Al-TCPPZn zn5aa", and cluster modeling compound 4 in this work "2DES@Al-TCPPZn zn7a".

At the single-point B3LYP/6-311G(d,p)+B3DJ level, the interaction energy of each DES molecule with Al-TCPPZn was -23.4 kcal/mol. This value is an overestimation due to the use of limited basis sets. When the counterpoise method of correcting the binding energy for Basis Set Superposition Error is incorporated [37 38], the binding energy is reduced by 4.5 kcal/mol to give a better estimate of -18.7 kcal/mol, Table 1. The BSSE-corrected binding energy in Table 1 of -18.7 kcal/mol indicates rather strong interaction of the DES molecules for the HOAl motif.

To our knowledge, there are no calculations of thermodynamics of sorption on DES on MOFs. There are limited reports on computing energy of adsorption of DES on "conventional" sorbents; Zhang et al. [9] used GCMC simulations to investigate evolution of co-adsorption of mixtures of diethyl sulfide with thiophene on Y zeolite. In [9] diethyl sulfide was more likely adsorbed on the Na^+ site; depending on the amount of competing co-adsorbate thiophene, the isosteric heat of adsorption of diethyl sulfide varies within 10-18 kcal/mol. In Table 1, the BE energy per DES molecule computed at the highly polar sorption site (DES-HOAl motif) is largely consistent with isosteric heat of adsorption of the same molecule at ionic Na^+ site in [9].

Additionally, the strong calculated interaction of DES with Al-TCPPZn in this work is consistent with an experimentally observed significant red shift in IR spectral peak of H-O-(Al) group in compound 3 after sorption of DES, see Figure 4a and 5a. In particular, in Figure 7 the distances S---HOAl are at 2.736 Å that indicates very strong interactions typical for hydrogen bonding involving electronegative atoms such as oxygen and sulfur [39]. The additional computed thermodynamic properties of reaction in Equation 2 are in Table 2.

Table 2. Estimate of the free energy of binding (ΔG(g,298K)) per DES molecule in the Al-TCPPZn model, in Equation 2 [a]

Thermodynamic property	Contribution to bonding	Numeric value, kcal/mol
ΔE	Electronic binding	-18.7
ZPC	Zero-point correction	-0.9
Cp	Heat capacity correction	-0.2
TΔS	Entropy correction to 298 K	+11.7
ΔG(g,298 K)	Binding per DES molecule	-6.3

a) The corrections are made using frequencies calculated at the B3LYP/6-31G(d)+D3BJ level. In order to compensate for the different number of imaginary frequencies of Al-TCPPZn cluster (1 imaginary frequency) and 2DES@Al-TCPPZn (3 imaginary frequencies), the contribution of two real modes to the entropy was ignored for the Al-TCPPZn cluster.

3.5) Kinetics of progressive sorption of DES vapor by compound 3, studied by *in-situ* time-dependent ATR-FTIR spectroscopy in controlled atmosphere

Before sorption of DES by compound 3 reaches equilibrium, it is desirable to determine sorption kinetics. The *in-situ* time-dependent ATR-FTIR spectroscopy was used to study dynamics of sorption of gases, but in the vast majority of cases the sorbent was used in the form of supported film e.g. [40]. Recently, we reported a new variant of *in-situ* time-dependent ATR-FTIR spectroscopy in controlled gaseous environment, where the sorbent is in physical form of powder [29]. In studies of kinetics of sorption, the Langmuir adsorption model is frequently used; see, for example, analytical and numerical solution of kinetics of sorption in the flow of a gas [41].

Figure 8b shows kinetic curve of sorption of DES vapor by compound 3: the integrated IR absorbance of characteristic vibration of DES (asymmetric CH_2 stretch) at 2965 cm^{-1} is shown versus time with kinetic analysis. Figure 8a shows the representative example of integration.

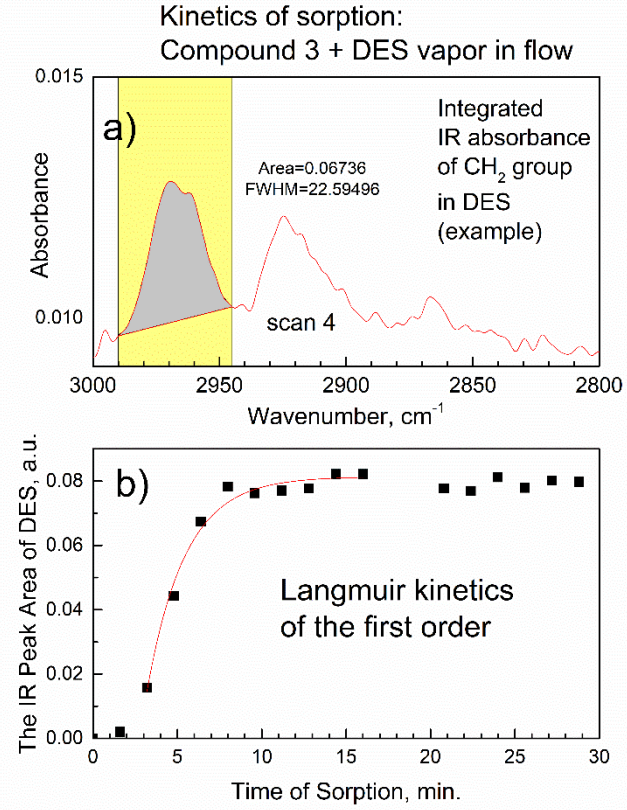

Figure 8. Kinetics of *in-situ* sorption of DES vapor by compound 3: a) representative example of integration of IR absorbance due to asymmetric CH_2 stretch at 2965 cm^{-1}; b) kinetic analysis of integrated absorbance vs time.

Here, we utilize kinetic analysis of dependence of integrated IR absorbance vs. time [42]. The formula of the Langmuir adsorption kinetics [43] of the pseudo-first order rate law is:

$$A_\nu(t) = b'(1 - \exp(-r_{obs}*t)) \quad (3)$$

where $A_\nu(t)$ is the integrated IR absorbance (area of peak with center at ν cm^{-1}), b' is empirical constant, r_{obs} is an observed (effective) kinetic rate constant, and t is sorption time. In Figure 8, kinetic analysis starts at time after zero, and the formula has a constant $A_\nu(offset)$ to account for it:

$$A_\nu(t) = A_\nu(offset) + b'(1 - \exp(-r_{obs}*t)) \quad (4)$$

The kinetic curve in Figure 8 is successfully fitted with equation (4) and a very good value is obtained for "goodness-of-fit" parameter R^2_{adj} = 0.978. The Langmuir adsorption kinetic rate constant of the pseudo-first order is $r_{obs} = 0.442 \pm 0.056$ min^{-1}.

After approximately 30 min. in the flow of DES vapor, the ATR-FTIR spectra remained the same. We attempted to regenerate "spent" sorbent in the spectroscopic mini-chamber from DES adsorbate i.e. under the same *in-situ* conditions. For this, the flow of DES vapor has been changed to dried air. The intensity of IR peaks of DES adsorbate in the sample has decreased, but not become zero. Hence, under the *in-situ* conditions, "spent" sorbent cannot be regenerated. Regeneration of "spent" sorbent under the ex-situ conditions is described in the next section.

3.6) Static sorption and desorption of DES vapor by compound 3

Sorption of DES vapor under the equilibrium (static) condition, in a closed desiccator filled with saturated DES vapor in dry air, yields the substantial mass increase of compound 3. Specifically, compound 3 Al-MOF-TCPPZn which has molecular formula $C_{48}H_{26}O_{10}N_4Al_2Zn$ undergoes the following process:

1 Al-MOF-TCPPZn (s) + 4 DES (vap) → $[\text{Al-MOF-TCPPZn}]_1(\text{DES})_4$ (s) (5)

Formation of the stoichiometric adsorption complex $[\text{Al-MOF-TCPPZn}]_1(\text{DES})_4$ (s) with four DES adsorbate molecules per one structural unit of sorbent compound 3 is consistent with the 3D structure of compound 3, which is a mesoporous MOF with very large lattice [30] parameters *a* = 31.8577(14) Å, *b* = 6.6002(3) Å, *c* = 16.8909(8) Å and volume = 3553.1(13) Å^3. Large mesopore in compound 3 readily allows localization of several DES molecules, which have the largest molecular dimension (estimated using ChemDraw 3D program) of only ca. 7 Å.

Figure 9 shows XRD pattern of adsorption complex of compound 3 after static sorption of DES vapor (Equation 5), in comparison with that of sorbent compound 3. The Y axis of the XRD pattern of the complex was proportionally scaled for better comparison. The two XRD patterns are mostly similar, indicating preservation of framework of compound 3 as sorbent and "host" material. However, some differences are present. First, for the adsorption complex, there is a new small peak at the angle 2θ = 10.8 deg. (marked with arrow in Figure 9). Similar effects were reported in studies of sorption of gases by MOFs; Saha et al. [44] reported that for mesoporous metal-organic framework MOF-5, the presence of adsorbate molecules in the nanopores results in a disappearance of one XRD peak, while other peaks remain.

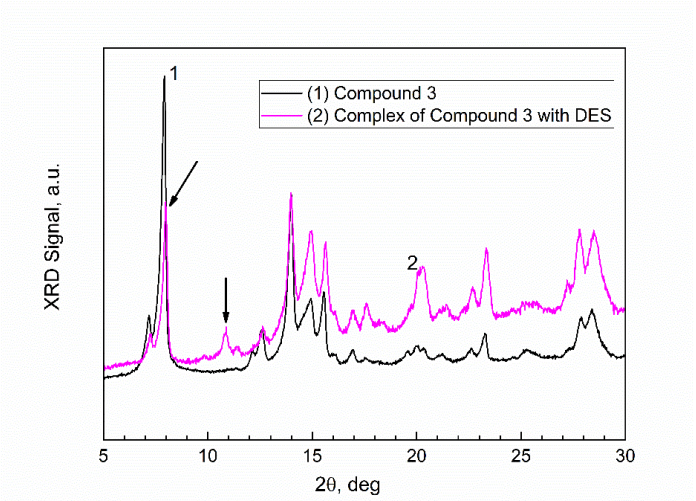

Figure 9. Powder XRD patterns of sorbent compound 3 and its adsorption complex with DES.

Second, one can see in Figure 9 the significant change in relative intensity of XRD peaks: major peak at 7.9 deg. (reflecting large inter-atomic distances in the framework) is significantly reduced after sorption (marked with arrow), while peaks at higher 2θ=13-16 deg. remain relatively high.

To our knowledge, this is the first report of sorption capacity of any MOF to diethyl sulfide. The adsorbed amount of DES by compound 3 is very high: 21.4 mg DES per 56.1 mg sorbent (38.1 wt. % or 381 mg/g sorbent). It is of interest to test the possibility of regeneration of this new sorbent. Figure 10 shows mass of sorbent compound 3 during "sorption/desorption" cycle.

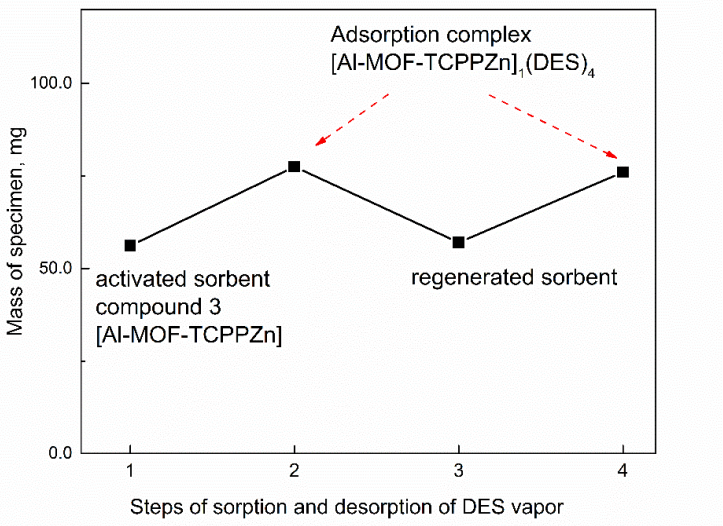

Figure 10. Gravimetric analysis of sorption and desorption of DES vapor by compound 3.

After sorption, "spent" sorbent was facilely regenerated in vacuum at room temperature to its initial mass. Compound 3 shows significant promise for removal of volatile organo-sulfur compounds by sorption in the vapor phase.

3.7) Assessment of molecular mechanism of bonding DES by compound 3 using Raman and photoluminescence spectroscopy

Figure S9 shows Raman spectra of compound 3 (in pure form), and compound 3 with added DES (see Experimental). After the interaction, peaks due to compound 3 do not change, but there is a significant growth of peak at 1445 cm^{-1} due to the deformation vibration of CH_3 group in DES molecule [34] as expected.

It is of interest to investigate the interaction of specific functional groups in linker of sorbent compound 3 with DES, using an additional method. The optics of confocal Raman microscope is capable of collecting spectra at very large Stokes shift up to about 13,000 cm^{-1}. This spectral range corresponds to wavelengths of light of up to 850 nm (red to near-infrared optical range).

Figure 11a shows the photoluminescence (PL) spectrum of compound 3 obtained using confocal Raman microscope at photoexcitation with laser at 405 nm (see Experimental). In Figure 11a and inset, Raman peaks of compound 3 are within ca. 70-2000 cm^{-1} as expected and consistently with Figure S9. Using Raman spectrometer for collection of photoluminescence (PL) spectra was reported in studies of semiconductors [45]. To our knowledge, this is the first report of the PL spectra of MOF recorded using confocal Raman microscope, or the Raman spectrometer.

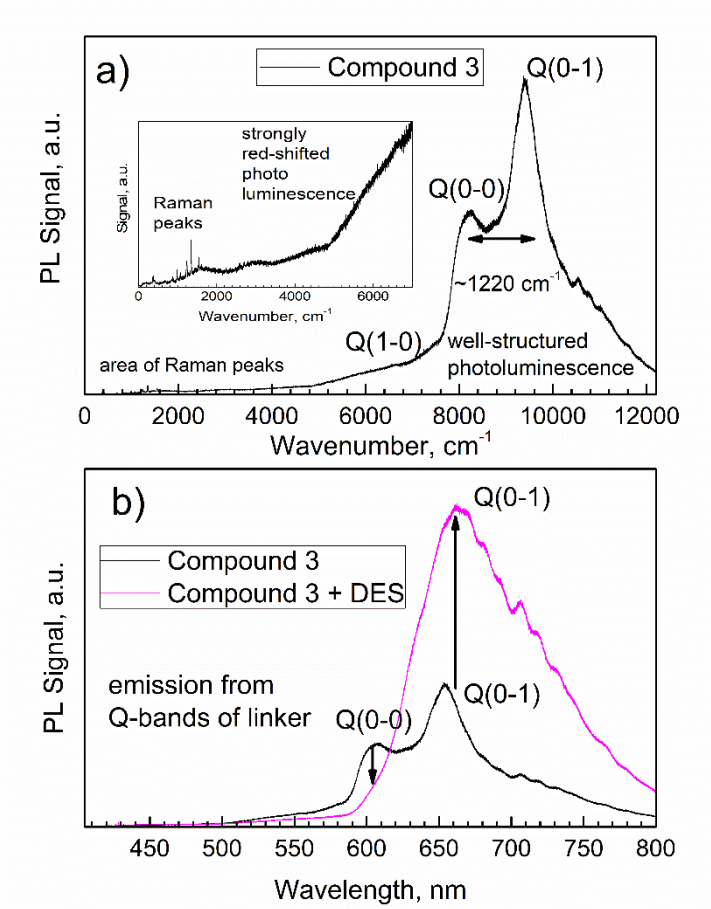

Figure 11. Photoluminescence (PL) spectral bands excited by the 405 nm laser of Raman microscope: a) sorbent compound 3; b) sorbent compound 3 with added DES.

In studies of optical properties of MOFs with metalloporphyrin linkers [46], emission spectra of MOFs are interpreted based on emission spectra of respective metalloporphyrin compounds. It is known that both porphyrins [19] and porphyrin linkers in MOFs [46] exhibit the photoluminescence (PL) in optical range ca. 550-800 nm, when the sample is photoexcited at the Soret band of metalloporphyrin at about 405 nm. The Zn-porphyrin unit in MOF compound 3 is the chromophore group responsible for optical absorption and emission.

In Figure 11a, the "fluorescence background" in Raman spectrum [47] is significant at ca. > 2000 cm^{-1}. At very large Raman shifts ca. 6,000-12,000 cm^{-1} this background is resolved into distinct photoluminescence (fluorescence) bands. Often, "fluorescence background" in Raman spectra is not desirable and techniques were developed for its suppression [48]. In contrast, there are examples of using well-structured optical emission bands collected in Raman spectroscopy experiment, to extract useful information about compounds [47]. In this work, Raman scattering peaks and PL bands excited by laser in the Raman instrument are well-resolved and synergistically complement each other. In Figure 11a one can see two well-defined PL peaks and shoulder.

In Figure 11b, these bands are re-plotted in wavelength domain and assigned. Porphyrins and metalloporphyrins have very strong absorption in 400–450 nm region (Soret band) and optical emission in visible to the NIR range of ca. 500–700 nm is structured into the Q-bands. For

metalloporphyrins ZnTCPP and ZnTPP, visible photoluminescence at ca. 560-700 nm is well-known [49] and the PL spectra consist of several Q-bands, Table 3.

Table 3. Photoluminescence peak maxima of compound 3 due to Q-bands of Zn-porphyrin linker.

The center wavelength λ of PL peaks in this work (compound 3), nm	The center λ of peaks in model ZnTCPP (literature), nm	The center λ of peaks in model ZnTPP (literature), nm	Assignment of PL peaks (literature)	Assignment of PL peaks of compound 3
ca. 574, broad band		560 a [50] 560 d [51]	Q(1-0) "hot band" [50, 51]	Q(1-0) aka "hot band"
607	610 c [19] 610 e [52]	605 b [50]	Q(0-0) purely electronic band [19, 50]	Q(0-0) band
653	658 c [19] 659 e [52]	647 a [50] 660 b [50]	Q(0-1) vibronic band [19, 50]	Q(0-1) vibronic band
>700 nm, broad tail		715 b [50] 781 b [50]	Q(0-2) and T(0-0) (phosphorescence)	Q(0-2) vibronic band and triplet states

a in benzene solution at room temperature [50]. b in frozen matrix (methylcyclohexane-isopentane) at 70 K [50]. c aqueous solution at room temperature [19]. d solution in ethanol [51]. e aqueous solution at room temperature [52]

In Figure 11a and Figure 11b, visible photoluminescence of compound 3 is due to luminescent Zn-porphyrin linker; in reference experiment pure DES did not give PL spectrum. In Figure 11b upon the interaction of compound 3 with DES, the initially strong PL emission from vibration-less Q(0-0) sublevel band of the linker is strongly quenched. Instead, PL emission from vibronic Q(0-1) sublevel is significantly enhanced. Index v = 0 indicates vibrational zeroths sublevel with vibrational quantum number v = 0 within electronic ground level S_0 (ground singlet state) and also within the first excited electronic level S_1 (the first excited singlet state). Similarly, index v = 1 corresponds to the first vibrationally excited sublevel (with vibrational quantum number v = 1) in the same electronic singlet states. The scheme of photoexcitation and relaxation is in Figure 12.

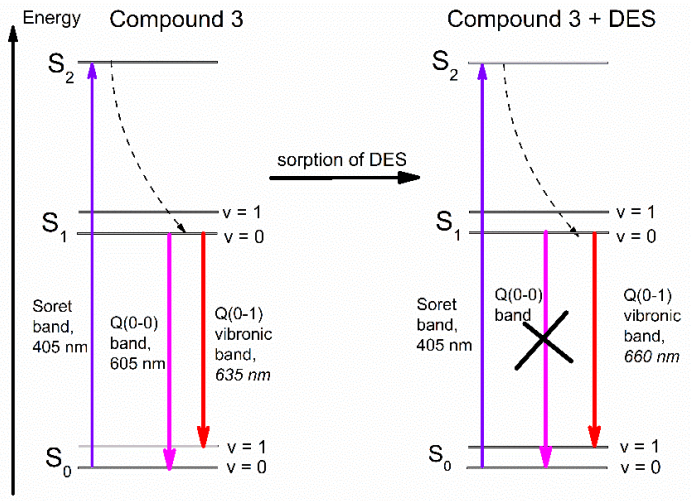

Figure 12. Scheme of photoexcitation and Q-band photoluminescence by Zn-porphyrin ring of linker in compound 3. Left (a): before sorption of DES; right (b): after sorption.

Preferential quenching of photoluminescence (i.e. electronic transition) from sorbent compound 3, originating in Zn-porphyrin ring of linker, indicates that DES molecules strongly interact with Zn-porphyrin ring. Quenching of PL (or fluorescence) from linker upon the interaction of the linker with adsorbate is often reported on studies of MOFs for optical sensing [53]. DES molecule has the sulfur atom with electron lone pairs, which is the "soft" Lewis base, while Zn^{2+} cation in Zn-porphyrin ring of linker is "soft" Lewis acid. Figure 13 shows the structure of binding site of DES molecule to compound 3 determined from the PL spectra.

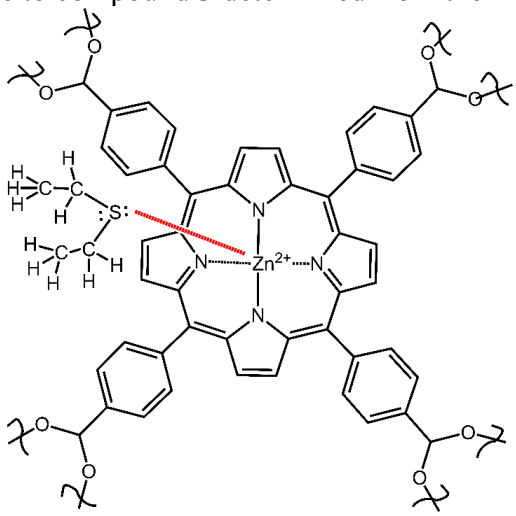

Figure 13. The second binding site of DES molecule to compound 3.

The intermolecular interaction in Figure 13 is favored by the planar structure of the metalloporphyrin ring of linker of compound 3. The PL spectra are very suitable for studies of sorption at this planar binding site of MOF, since vibronic Q(0-1) band reflects vibrations of atoms in Zn-porphyrin ring and the S atom of DES molecule interacting with it. On the other hand, it would be not easy to detect vibrations of atoms in Zn-porphyrin ring in ATR-FTIR spectra, since these are coupled vibrations in the low wavenumbers range, where unambiguous assignments of

IR peaks are difficult. Additionally, the affected bonds in Figure 13 are only weakly polar and hence correspond to IR peaks of low absorbance, per quantum selection rules.

Figure 6 shows the structure of another binding site at the polar μ(OH) and carboxylate group in compound 3, determined by *in-situ* time-dependent ATR-FTIR spectra in controlled atmosphere. The IR spectroscopy is very suitable for detection of binding DES adsorbate at polar OH and COO^- group, due to selection rules of IR spectroscopy, where polar bonds are well detected. The existence of two bonding sites of DES molecules in sorbent compound 3 is consistent with the stoichiometry of adsorption complex [Al-MOF-TCPPZn](DES)$_4$ where one structural unit of MOF contains as many as four molecules of DES adsorbate. Due to symmetry of the linker, it is possible that two DES molecules are interacting with (Al)-O-H and COO^- groups and other two with TCPPZn ring of linker. Further studies of fine mechanistic details of different modes of binding of multiple adsorbate molecules to more than one sorption site is outside of this work. On the other hand, the PL quenching of Q-band in compound 3 upon interaction with DES opens the road to potential applications of compound 3 for chemo-sensing DES and similar VOSCs, based on facile and straightforward optical method of photoluminescence.

Conclusions

This work reports mechanistic study of interactions between sorbent zinc-containing porphyrin aluminum MOF (compound 3) and volatile organic sulfur compound diethyl sulfide (DES), conducted by the combination of multiple complementary *in-situ* and *ex-situ* experimental methods and DFT computations. First, studies under dynamic sorption conditions, namely with vapor of DES in flowing dried air, conducted by *in-situ* time-dependent ATR-FTIR spectroscopy in controlled atmosphere and by using new facilely made spectroscopic mini-chamber, reveal specific binding sites in compound 3. They are the μ(O-H) and COO^- groups in the linker detected through their characteristic IR peak shifts upon gradual sorption of DES. The control experiments with non-porous model compound ZnTCPP, that lacks nanoporosity and these groups, show no spectral shifts. Second, the molecular mechanism of interaction of compound 3 with DES adsorbate was assessed by quantum chemical DFT computations. Third, chemical kinetics of sorption of DES by compound 3 is found to follow the Langmuir adsorption model, with the pseudo-first order rate law and effective kinetic rate constant $r_{obs} = 0.442 \pm 0.056$ min^{-1}. Fourth, sorption of DES vapor by compound 3 under the equilibrium conditions (in saturated vapor) results in the stoichiometric adsorption complex [Al-MOF-TCPPZn]$_1$(DES)$_4$. This stoichiometry corresponds to a very high adsorbed amount of DES at 381 mg/g sorbent. Fifth, the repetitive sorption and desorption of DES vapor by compound 3 was conducted, with facile regeneration of "spent" sorbent which makes possible its reuse for sorption of DES. Sixth, multiple molecules of DES adsorbate present in the secondary building unit of MOF compound 3 imply existence of more than one modality of their interaction with sorption sites in this sorbent. Here, mechanistic details of these interactions were obtained using a novel approach – the photoluminescence (PL) spectra collected using confocal Raman microscope, att the resonant photoexcitation into the Soret band of Zn-porphyrin linker of compound 3. The photoexcitation with laser at 405 nm into the Soret band shows the two characteristic PL peaks of Q-bands of Zn-porphyrin: the purely electronic Q(0-0) band and the first vibronic Q(0-1) band. Interestingly, upon interaction with DES, the preferential quenching of the Q(0-0) band is observed, with the concurrent enhancement of the Q(0-1) vibronic band, attributed to interaction of DES adsorbate with Zn-porphyrin ring as the second binding site in compound 3. Zinc-containing porphyrin aluminum MOF compound 3 is of interest to mechanistic studies of molecular interactions with volatile organic sulfur

compounds (VOSCs) including diethyl sulfide. Additionally, it is a promising advanced sorbent for removal of VOSCs from air, and it may find applications in chemo-sensing these toxic compounds using facile optical detection method.

Acknowledgement

Research was sponsored by the Army Research Office and was accomplished under Grant Number W911NF-20-1-0290. The views and conclusions contained in this document are those of the authors and should not be interpreted as representing the official policies, either expressed or implied, of the Army Research Office or the U.S. Government. The U.S. Government is authorized to reproduce and distribute reprints for Government purposes notwithstanding any copyright notation herein.

Research was sponsored by the Army Research Office and was accomplished under the Instrumentation Grant Number W911NF-21-1-0204, titled "Acquisition of Advanced Vibrational and Optical Spectroscopy and Imaging System for Interdisciplinary Materials Research, STEM Education, and Outreach".

The Easley supercomputer at Auburn University is acknowledged for providing computer resources.

References

[1] T.G. Chasteen and R. Bentley, Volatile organic sulfur compounds of environmental interest: Dimethyl sulfide and methanethiol. An introductory overview, *J. Chem. Educ.*, 2004, **81**, 1524.

[2] T. Wu, T. Wu, X. Wang, D. Li and Z. Yi, Emission of volatile organic sulfur compounds (VOSCs) during aerobic decomposition of food wastes, *Atmos. Environ.*, 2010, **44**, 5065-5071.

[3] D.T. McAllan, T.V. Cullum, R.A. Dean and F.A. Fidler, The preparation and properties of sulfur compounds related to petroleum. I. The dialkyl sulfides and disulfides1, *J. Am. Chem. Soc.*, 1951, **73**, 3627-3632.

[4] L. Wenjing, D. Zhenhan, L. Dong, L.M.C. Jimenez, L. Yanjun, G. Hanwen and W. Hongtao, Characterization of odor emission on the working face of landfill and establishing of odorous compounds index, *Waste Manag.*, 2015, **42**, 74-81.

[5] B. Zang, S. Li, F. Michel, Jr., G. Li, Y. Luo, D. Zhang and Y. Li, Effects of mix ratio, moisture content and aeration rate on sulfur odor emissions during pig manure composting, *Waste Manag.*, 2016, **56**, 498-505.

[6] C. Ramakrishna, S.C. Shekar, A.K. Gupta, B. Saini, R. Krishna, G. Swetha and T. Gopi, Degradation of diethyl sulfide vapors with manganese oxide catalysts supported on zeolite-13X: The influence of process parameters and mechanism in presence of ozone, *J. Environ. Chem. Eng.*, 2017, **5**, 1484-1493.

[7] A.J. Howarth, C.T. Buru, Y. Liu, A.M. Ploskonka, K.J. Hartlieb, M. McEntee, J.J. Mahle, J.H. Buchanan, E.M. Durke, S.S. Al-Juaid, J.F. Stoddart, J.B. DeCoste, J.T. Hupp and O.K. Farha, Postsynthetic incorporation of a singlet oxygen photosensitizer in a metal–organic framework for fast and selective oxidative detoxification of sulfur mustard, *Chem. Eur. J.*, 2017, **23**, 214-218.

[8] G.K. Prasad, B. Singh, U.V.R. Saradhi, M.V.S. Suryanarayana and D. Pandey, Adsorption and reaction of diethyl sulfide on active carbons with and without impregnants under static conditions, *Langmuir*, 2002, **18**, 4300-4306.

[9] G. Zhang, P. Xue, J. Wei, Y. Zhang, L. Zhao, J. Gao and C. Xu, Competitive adsorption mechanism of thiophene with diethyl sulfide in Y zeolite: Displacement and migration, *Chem. Eng. J.*, 2022, **435**.

[10] A. Samokhvalov, Adsorption on mesoporous metal-organic frameworks in solution for clean energy, environment and healthcare, CRC Press, Boca Raton, FL, USA, 2017.
[11] Z. Hasan and S.H. Jhung, Removal of hazardous organics from water using metal-organic frameworks (MOFs): Plausible mechanisms for selective adsorptions, *J. Hazard. Mater.*, 2015, **283**, 329-339.
[12] W.P. Lustig, S. Mukherjee, N.D. Rudd, A.V. Desai, J. Li and S.K. Ghosh, Metal–organic frameworks: Functional luminescent and photonic materials for sensing applications, *Chem. Soc. Rev.*, 2017, **46**, 3242-3285.
[13] V.R. Remya and M. Kurian, Synthesis and catalytic applications of metal–organic frameworks: A review on recent literature, *Int. Nano Lett.*, 2019, **9**, 17-29.
[14] A.J. Rieth, A.M. Wright and M. Dincă, Kinetic stability of metal–organic frameworks for corrosive and coordinating gas capture, *Nat. Rev. Mater.*, 2019, **4**, 708-725.
[15] J.E. Mondloch, M.J. Katz, W.C. Isley Iii, P. Ghosh, P. Liao, W. Bury, G.W. Wagner, M.G. Hall, J.B. DeCoste, G.W. Peterson, R.Q. Snurr, C.J. Cramer, J.T. Hupp and O.K. Farha, Destruction of chemical warfare agents using metal–organic frameworks, *Nat. Mater.*, 2015, **14**, 512–516.
[16] A. Samokhvalov, Aluminum metal–organic frameworks for sorption in solution: A review, *Coord. Chem. Rev.*, 2018, **374**, 236-253.
[17] B. Henry and A. Samokhvalov, Hygroscopic metal-organic framework MIL-160(Al): In-situ time-dependent ATR-FTIR and gravimetric study of mechanism and kinetics of water vapor sorption, *Spectrochim. Acta A*, 2022, **267**, Article 120550.
[18] C. Wang, B. Liu, F. Sun, J. Xie and Q. Pan, New challenge of microporous metal-organic frameworks for adsorption of hydrogen fluoride gas, *Mater. Lett.*, 2017, **197**, 175-179.
[19] K. Kalyanasundaram and M. Neumann-Spallart, Photophysical and redox properties of water-soluble porphyrins in aqueous media, *J. Phys. Chem.*, 1982, **86**, 5163-5169.
[20] S. Nakashima, R. Negishi and H. Tada, Visible-light-induced water oxidation by a hybrid photocatalyst consisting of bismuth vanadate and copper(II) meso-tetra(4-carboxyphenyl)porphyrin, *Chem. Commun.*, 2016, **52**, 3665-3668.
[21] C. Fu, X. Sun, G. Zhang, P. Shi and P. Cui, Porphyrin-based metal–organic framework probe: Highly selective and sensitive fluorescent turn-on sensor for M3+ (Al3+, Cr3+, and Fe3+) ions, *Inorg. Chem.*, 2021, **60**, 1116-1123.
[22] Z. Safaei Moghaddam, M. Kaykhaii, M. Khajeh and A.R. Oveisi, Application of an iron-based porphyrinic metal–organic framework for removal of warfarin from aqueous solutions, *Anal. Methods*, 2020, **12**, 651-656.
[23] K.C. Wang, D.W. Feng, T.F. Liu, J. Su, S. Yuan, Y.P. Chen, M. Bosch, X.D. Zou and H.C. Zhou, A series of highly stable mesoporous metalloporphyrin Fe-MOFs, *J. Am. Chem. Soc.*, 2014, **136**, 13983-13986.
[24] J.A. Harvey, M.L. McEntee, S.J. Garibay, E.M. Durke, J.B. DeCoste, J.A. Greathouse and D.F. Sava Gallis, Spectroscopically resolved binding sites for the adsorption of sarin gas in a metal–organic framework: Insights beyond Lewis acidity, *J. Phys. Chem. Lett.*, 2019, **10**, 5142-5147.
[25] G.-A. Banga-Bothy and A. Samokhvalov, Porphyrin aluminum mof with ultra-high water sorption capacity: In-situ time-dependent ATR-FTIR spectroscopy and gravimetry to study mechanism of water bonding and desorption, *Vib. Spectrosc.*, 2022, **119**, Article 103356.
[26] S.G. Kazarian, M.F. Vincent and C.A. Eckert, Infrared cell for supercritical fluid–polymer interactions, *Rev. Sci. Instrum.*, 1996, **67**, 1586-1589.

[27] I.P. Silverwood, C.W. Keyworth, N.J. Brown, M.S.P. Shaffer, C.K. Williams, K. Hellgardt, G.H. Kelsall and S.G. Kazarian, An attenuated total reflection fourier transform infrared (ATR FT-IR) spectroscopic study of gas adsorption on colloidal stearate-capped ZnO catalyst substrate, *Appl. Spectrosc.*, 2014, **68**, 88-94.
[28] D. Guerra, L. Ricciardi, J.-C. Laborde and S. Domenech, Predicting gaseous pollutant dispersion around a workplace, *J. Occup. Environ. Hyg.*, 2007, **4**, 619-633.
[29] A. Samokhvalov and S. McCombs, In situ time-dependent attenuated total reflection fourier transform infrared (ATR FT-IR) spectroscopy of a powdered specimen in a controlled atmosphere: Monitoring sorption and desorption of water vapor, *Appl. Spectrosc.*, 2023, **77**, 308-319.
[30] A. Fateeva, P.A. Chater, C.P. Ireland, A.A. Tahir, Y.Z. Khimyak, P.V. Wiper, J.R. Darwent and M.J. Rosseinsky, A water-stable porphyrin-based metal–organic framework active for visible-light photocatalysis, *Angew. Chem. Int. Ed.*, 2012, **51**, 7440-7444.
[31] M.J. Frisch, G.W. Trucks, H.B. Schlegel, G.E. Scuseria, M.A. Robb, J.R. Cheeseman, G. Scalmani, V. Barone, G.A. Petersson, H. Nakatsuji, X. Li, M. Caricato, A.V. Marenich, J. Bloino, B.G. Janesko, R. Gomperts, B. Mennucci, H.P. Hratchian, J.V. Ortiz, A.F. Izmaylov, J.L. Sonnenberg, D. Williams-Young, F. Ding, F. Lipparini, F. Egidi, J. Goings, B. Peng, A. Petrone, T. Henderson, D. Ranasinghe, V.G. Zakrzewski, J. Gao, N. Rega, G. Zheng, W. Liang, M. Hada, M. Ehara, K. Toyota, R. Fukuda, J. Hasegawa, M. Ishida, T. Nakajima, Y. Honda, O. Kitao, H. Nakai, T. Vreven, K. Throssell, J.A. Montgomery, Jr., J.E. Peralta, F. Ogliaro, M.J. Bearpark, J.J. Heyd, E.N. Brothers, K.N. Kudin, V.N. Staroverov, T.A. Keith, R. Kobayashi, J. Normand, K. Raghavachari, A.P. Rendell, J.C. Burant, S.S. Iyengar, J. Tomasi, M. Cossi, J.M. Millam, M. Klene, C. Adamo, R. Cammi, J.W. Ochterski, R.L. Martin, K. Morokuma, O. Farkas, J.B. Foresman and D.J. Fox, Gaussian 16 revision b. 01, *Gaussian, Inc.*, 2016, Wallingford, CT.
[32] M.L. McKee and A. Samokhvalov, Interactions of multiple water molecules with MIL-53(Al) and understanding the mechanism of breathing: The DFT study, *J. Phys. Chem. C*, 2020, **124**, 9281-9288.
[33] J.I. Langford and A.J.C. Wilson, Scherrer after sixty years: A survey and some new results in the determination of crystallite size, *J. Appl. Crystallogr.*, 1978, **11**, 102-113.
[34] S.D. Christesen, Vibrational spectra and assignments of diethyl sulfide, 2-chlorodiethyl sulfide and 2, 2′-dichlorodiethyl sulfide, *J. Raman Spectrosc.*, 1991, **22**, 459-465.
[35] R.W. Glass and R.A. Ross, Surface studies of the adsorption of sulfur-containing gases at 423.Deg.K on porus adsorbents. II. Adsorption of hydrogen sulfide, methanethiol, ethanethiol, and dimethyl sulfide on gamma-alumina, *J. Phys. Chem.*, 1973, **77**, 2576-2578.
[36] S. Tsuzuki and T. Uchimaru, Accuracy of intermolecular interaction energies, particularly those of hetero-atom containing molecules obtained by DFT calculations with grimme's D2, D3 and D3Bj dispersion corrections, *Phys. Chem. Chem. Phys.*, 2020, **22**, 22508-22519.
[37] F.B. van Duijneveldt, J.G.C.M. van Duijneveldt-van de Rijdt and J.H. van Lenthe, State of the art in counterpoise theory, *Chem. Rev.*, 1994, **94**, 1873-1885.
[38] Á. Vidal Vidal, L.C. de Vicente Poutás, O. Nieto Faza and C. Silva López, On the use of popular basis sets: Impact of the intramolecular basis set superposition error, *Molecules*, 2019, **24**, 3810.
[39] T.K. Harris and A.S. Mildvan, High-precision measurement of hydrogen bond lengths in proteins by nuclear magnetic resonance methods, *Proteins*, 1999, **35**, 275-282.
[40] R.T. Woodward, L.A. Stevens, R. Dawson, M. Vijayaraghavan, T. Hasell, I.P. Silverwood, A.V. Ewing, T. Ratvijitvech, J.D. Exley, S.Y. Chong, F. Blanc, D.J. Adams, S.G. Kazarian, C.E.

Snape, T.C. Drage and A.I. Cooper, Swellable, water- and acid-tolerant polymer sponges for chemoselective carbon dioxide capture, *J. Am. Chem. Soc.*, 2014, **136**, 9028-9035.
[41] R.D. Brancher, S. Stefanov, I. Graur and A. Frezzotti, A kinetic model for gas adsorption-desorption at solid surfaces under non-equilibrium conditions, *Vacuum*, 2020, **174**, 109166.
[42] E. Possenti, C. Colombo, M. Realini, C.L. Song and S.G. Kazarian, Time-resolved ATR-FTIR spectroscopy and macro ATR-FTIR spectroscopic imaging of inorganic treatments for stone conservation, *Anal. Chem.*, 2021, **93**, 14635-14642.
[43] J. Tofan-Lazar and H.A. Al-Abadleh, Kinetic ATR-FTIR studies on phosphate adsorption on iron (oxyhydr)oxides in the absence and presence of surface arsenic: Molecular-level insights into the ligand exchange mechanism, *J. Phys. Chem. A*, 2012, **116**, 10143-10149.
[44] D. Saha, S. Deng and Z. Yang, Hydrogen adsorption on metal-organic framework (MOF-5) synthesized by DMF approach, *J. Porous Mater.*, 2009, **16**, 141-149.
[45] H. Liu and D. Chi, Dispersive growth and laser-induced rippling of large-area single layer MoS2 nanosheets by CVD on c-plane sapphire substrate, *Sci. Rep.*, 2015, **5**, 11756.
[46] S.S. Rajasree, X. Li and P. Deria, Physical properties of porphyrin-based crystalline metal–organic frameworks, *Commun. Chem.*, 2021, **4**, 47.
[47] T. Buchwald, Z. Buchwald and A. Daktera-Micker, The fluorescence background in Raman spectra of sound enamel, *Vib. Spectrosc.*, 2021, **115**, 103275.
[48] D. Wei, S. Chen and Q. Liu, Review of fluorescence suppression techniques in Raman spectroscopy, *Appl. Spectrosc. Rev.*, 2015, **5**, 387-406.
[49] T. Hashimoto, Y.-K. Choe, H. Nakano and K. Hirao, Theoretical study of the Q and B bands of free-base, magnesium, and zinc porphyrins, and their derivatives, *J. Phys. Chem. A*, 1999, **103**, 1894-1904.
[50] D.J. Quimby and F.R. Longo, Luminescence studies on several tetraarylporphins and their zinc derivatives, *J. Am. Chem. Soc.*, 1975, **97**, 5111-5117.
[51] N. Mataga, Y. Shibata, H. Chosrowjan, N. Yoshida and A. Osuka, Internal conversion and vibronic relaxation from higher excited electronic state of porphyrins: Femtosecond fluorescence dynamics studies, *J. Phys. Chem. B*, 2000, **104**, 4001-4004.
[52] M. Ravikant, D. Reddy and T.K. Chandrashekar, Dimerization effects on spectroscopic properties of water-soluble porphyrins in aqueous and micellar media, *J. Chem. Soc., Dalton Trans.*, 1991, 2103-2108.
[53] J. Yang, Z. Wang, K. Hu, Y. Li, J. Feng, J. Shi and J. Gu, Rapid and specific aqueous-phase detection of nitroaromatic explosives with inherent porphyrin recognition sites in metal–organic frameworks, *ACS Appl. Mater. Interfaces*, 2015, **7**, 11956-11964.